Visualization of Oleic Acid-induced Transdermal Diffusion Pathways Using Two-photon Fluorescence Microscopy

Betty Yu, Ki Hean Kim,* Peter T. C. So,* Daniel Blankschtein, and Robert Langer

Department of Chemical Engineering, Massachusetts Institute of Technology, Cambridge, MA 02139, U.S.A.; *Department of Mechanical Engineering, Massachusetts Institute of Technology, Cambridge, MA 02139, U.S.A.

In a novel application of dual-channel high-speed two-photon fluorescence microscopy, the skin autofluorescence and the transdermal fluorescent model drug spatial distributions were imaged simultaneously over precisely the same spatial coordinates. The dual channels enable the detection of the fluorescence emission wavelengths characteristic of the endogenous (intrinsic) skin fluorophores, as well as of the rhodamine-based model drug intensity emission at a different wavelength range of the fluorescence emission spectrum. These fluorescent model drugs delineate the oleic acid induced changes in permeant diffusion with respect to the skin structural features over the 0.3 mm by 0.3 mm skin area imaged per skin sample. The dual-channel high-speed two-photon fluorescence microscopy studies presented here provide evidence for the existence of intracorneocyte diffusion in addition to the commonly cited lipid multilamellar transdermal pathway. The image quantification analysis methodology introduced in this paper reveals that intracorneocyte diffusion exists for the hydrophobic (rhodamine B hexyl ester) and for the hydrophilic (sulforhodamine B) model drugs, in the absence of oleic acid chemical enhancer action. The mechanism of oleic acid chemical enhancer action, however, depends on the model drug physicochemical properties, where the oleic acid induces hydrophobic model drug localization to the lipid multilamellar region, while increasing the hydrophilic model drug lipid to corneocyte partitioning. ***Key words: chemical enhancement mechanism/dual-channel high-speed two-photon fluorescence microscopy/oleic acid/skin autofluorescence. J Invest Dermatol 120:448–455, 2003***

The advantages of using two-photon fluorescence microscopy to examine a highly scattering and morphologically complex system, such as the skin have been described previously (Masters *et al*, 1997, 1998; Diaspro, 1999; Soeller and Cannell, 1999; Yu *et al*, 2001), where some of the advantages include reduced sample photobleaching and increased three-dimensional depth discrimination. The evaluation of oleic acid-induced transdermal transport has focused in the past on the primary diffusion pathway associated with the intercellular lipid region that was well delineated by both the hydrophobic and the hydrophilic model drugs (Gerritsen and de Grauw, 1999; Yu *et al*, 2002). In this paper, we address the role of the corneocytes within the complex stratum corneum (SC) structure in the case of oleic acid-induced transdermal transport.

Until now, the study of chemical enhancer action has focused primarily on the alteration of the SC barrier properties resulting from a fluidization of the lipid multilamellar region through which the permeants diffuse (Golden *et al*, 1986, 1987). The increased lipid disorder resulting from lipid fluidization has been cited as being responsible for the increase in drug partitioning into the SC, as well as for the increase in the porosity of the SC membrane (Yamashita *et al*, 1995; Yoneto *et al*, 1998). Although chemical enhancer-induced deformation of the corneocytes has been described in studies using octyl glucoside (Lopez *et al*, 2000a, b), the role of the corneocyte structures in transdermal transport processes has been largely neglected, primarily due to their relative impermeability when compared with that of the lipid multilamellar region (Matoltsy, 1976).

As a new approach to identify the oleic acid-induced changes in intracorneocyte model drug penetration, a dual-channel high-speed two-photon fluorescence microscope (HTPM), used to filter the fluorescence emission wavelengths in the green color spectrum range from the red color spectrum range, enables the simultaneous visualization of the fluorescence signals resulting from the intrinsic skin autofluorescence in one channel and those signals resulting from the exogenous (or externally introduced) fluorescent model drug in the second channel. In current studies available in the literature (Grewal *et al*, 2000; Yu *et al*, 2001, 2002), the exogenous model drug fluorescence was examined without evaluating the corresponding skin autofluorescence image. Hence, the fluorescent model drug spatial coordinates were evaluated without a visualization of the underlying SC structural features that govern the model drug diffusion pathways. In this paper, we characterize the exogenous model drug spatial distributions in the skin with respect to the intrinsic skin autofluorescence at precisely the same skin spatial coordinates.

Skin autofluorescence has been well studied in the literature, both *in vivo* and *in vitro* (Kollias *et al*, 1998; Gonzalez *et al*, 2000; Na *et al*, 2001). Using excitation wavelengths ranging from

Manuscript received July 17, 2002; revised November 2, 2002; accepted for publication November 5, 2002

Reprint requests to: Daniel Blankschtein, Department of Chemical Engineering, Room 66-444, Massachusetts Institute of Technology, 77 Massachusetts Avenue, Cambridge, MA 02139-4307, U.S.A. Email: dblank@mit.edu

Abbreviations: DHTPM, dual-channel high-speed two-photon microscopy; SC, stratum corneum; RBHE, rhodamine B hexyl ester; SRB, sulforhodamine B.

340 nm to 380 nm, the skin autofluorescence emission spectrum was detected using a fluorescence spectrophotometer that revealed two major component bands centered at 450 nm and 520 nm, that corresponded to 75% and 25% of the total spectrum intensity, respectively (Na *et al*, 2000). These two peaks in the skin autofluorescence spectrum correspond to the fluorescence emission peaks of the endogenous (or intrinsic) skin fluorophores, that include collagen, elastin, aromatic amino acids, such as tryptophan and tyrosine, nicotinamideadenine dinucleotide, porphyrins, and flavin adenine dinucleotide (Kollias *et al*, 1998). The structural details of the corneocyte–lipid interface, delineated by imaging the intrinsic skin autofluorescence, enables the quantitation of model drug spatial distributions relative to the corneocyte structures in the same skin sample, at precisely the same spatial locations.

MATERIALS AND METHODS

Skin sample preparation Using the methodology described previously (Yu *et al*, 2001, 2002) excised human cadaver skin (National Disease Research Interchange, Philadelphia, PA) was mounted in side-by-side diffusion cells (Permegear, Riegelsville, PA). The model drug control and enhancer vehicle solutions consisted of 50/50 v/v phosphate-buffered saline/ethanol and of the control solution containing an additional 5% oleic acid (Sigma, St Louis, MO), respectively. The hydrophobic and the hydrophilic model drug concentrations of rhodamine B hexyl ester (RBHE) and sulforhodamine B (SRB) (Molecular Probes, Eugene, OR), respectively, were adjusted such that the exogenous fluorescent model drug intensity signal detected was comparable with the endogenous SC autofluorescence intensity. The dilution of the RBHE and SRB vehicles to 0.005 mg per ml (compared with the 0.33 mg per ml utilized in the studies reported previously; Yu *et al*, 2001, 2002) enables the simultaneous imaging of the skin autofluorescence as well as of the exogenous fluorescent model drug intensities, such that model drug signal saturation is avoided. After 24 h of skin exposure to the model drug solution, the samples were rinsed with phosphate-buffered saline, and mounted on microscope slides as described previously (Yu *et al*, 2002).

HTPM A detailed description of the HTPM methodology utilized in these studies can be found in the literature (Kim *et al*, 1999). Modifications to the HTPM instrumentation include the use of a filter set (Chroma Technologies, Brattleboro, VT) that separates the fluorescence emission signal into two wavelength ranges. The filter set consists of a dichroic mirror (part no. 530DCXR), a short pass filter (part no. E535SP), and a bandpass filter (part no. D630/40). The dichroic mirror reflects emission wavelengths below 530 nm to one channel, where the short pass filter is applied. Fluorescence emission signals in the range of 610 nm to 650 nm, that are reflected from the dichroic mirror, are detected in the second channel using the bandpass filter. The first channel collects the emission wavelengths characteristic of the intrinsic skin fluorophores, and will be referred to as the green channel. The second channel, or the red channel, detects the model drug fluorescence signal (**Table I** lists the absorption and emission wavelengths of each model drug). The model drug spatial distributions in the following studies were evaluated in nine consecutive skin sites, each skin site having an area of 100 μm by 100 μm.

At the laser power used, the skin autofluorescence intensities treated with the control and the enhancer vehicle solutions in the presence and in the absence of the model drugs are comparable. This comparison of the skin autofluorescence intensities verifies that the skin autofluorescence signal detected in the green channel arises from the endogenous skin fluorophores, and not from signal noise introduced by the model drugs.

Table I. Fluorescent model drug properties of the hydrophobic (RBHE) and the hydrophilic (SRB) model drugs examined.[a]

Probe	RBHE	SRB
MW (Da)	627	559
ab/em (nm)	556/578	565/586
log $K^{b}_{O/PBS}$	2.49 ± 0.18	$-0.45 \pm .0045$

[a]MW is the molecular weight of each probe; ab/em indicates the probe spectral absorption (ab) and emission peaks (em); $logK_{O/PBS}$, reflects the measured values of the log of the probe PBS-octanol partition coefficients (Yu *et al.*, 2001).

[b]Values are reported as mean ± SD. Experiments were performed in triplicate

Image analysis of model drug spatial distributions To elucidate the role of intracorneocyte diffusion in transdermal transport, nine consecutive skin sites (600×600 pixels in image size) representative of a continuous skin region containing well defined, regularly spaced corneocytes, were selected for each skin sample. To focus on the SC structural dimensions defined by the skin autofluorescence and by the model drug intensity signals, a representative subregion, spanning 150×150 pixels, was selected from the total 600×600 pixels skin image acquired for each condition: RBHE-control, RBHE-enhancer, SRB-control, and SRB-enhancer. Within each 150×150 pixel image, a linear path of 5 pixels in width (y coordinate) and 150 pixels in length (x coordinate) was deconstructed into its pixel intensity values to determine the intercellular region width, defined by the fluorescence intensity peak widths. At each position along the x coordinate, the intensities of the corresponding 5 pixels were averaged. The arbitrarily selected line width of 5 pixels accounts for the intensity variations along the y coordinate while limiting the inclusion of intensities arising from different structural features in the average value. The resulting plot of the fluorescence intensity spectrum for the green channel, as a function of the x coordinate position, reveals the peak-to-peak distance as well as the peak width, which indicate the corneocyte width and the intercellular spacing, respectively, along the 150 pixel linear region analyzed. The corresponding plot of the model drug fluorescence intensity spectrum for the red channel describes the model drug spatial distribution relative to the skin structural features defined by the skin autofluorescence intensity spectrum. These skin autofluorescence and model drug intensity spectra are then normalized with respect to the corresponding maximum fluorescence intensities detected within the selected linear path. Because the skin autofluorescence and the model drug fluorescence signals span two different intensity ranges, the fluorescence intensity normalization enables a comparison of the relative changes in the spatial intensity distributions between these two fluorescence intensity signals using the same normalized scale, where zero values reflect the absence of a fluorescence intensity signal and values of 1 represent maximum fluorescence intensity signals.

RESULTS AND DISCUSSION

Visualization of fluorescent model drug spatial distributions The HTPM dual-channel imaging visualizations of the skin autofluorescence and of the exogenous model drug intensity are presented in **Figs 1 and 2** for the hydrophobic model drug RBHE and for the hydrophilic model drug SRB, respectively.

Hydrophobic model drug (RBHE) The black regions that are surrounded by the green intercellular autofluorescence depict the corneocyte structures for the control case (see **Fig 1*a***). Based on the length of the 100 μm scale bar provided at the lower left of **Fig 1(*a*)**, the corneocyte dimensions are approximately 30 μm, which is consistent with the 30–40 μm diameter reported in the literature (Heisig *et al*, 1996).

A comparison of the skin autofluorescence image for the control RBHE case (**Fig 1*a***) with the RBHE-control model drug spatial distribution (**Fig 1*b***) indicates that RBHE primarily traverses the intercellular region. In the overlay of the green and the red channels shown in **Fig 1(*c*)**, a majority of the RBHE signal is observed to be positioned within the intercellular space delineated by the skin autofluorescence. In **Fig 1(*b*)**, the corneocyte structures exhibit a lower fluorescence intensity compared with the intercellular lipid multilamellar region model drug intensity, located at the perimeter of the corneocyte structures. This finding is consistent with previous studies using HTPM aimed at elucidating the mechanisms of chemical enhancer action (Yu *et al*, 2002). The visualization of RBHE model drug fluorescence within the periphery of the corneocyte structures, however, indicates that intracorneocyte diffusion may result from the fluorescent model drug concentration difference between the intercellular region and the fluorescent model drug deficient corneocyte interior.

The oleic acid-induced changes in the RBHE spatial distribution are observed upon comparing **Fig 1(*d*,*e*)**. The

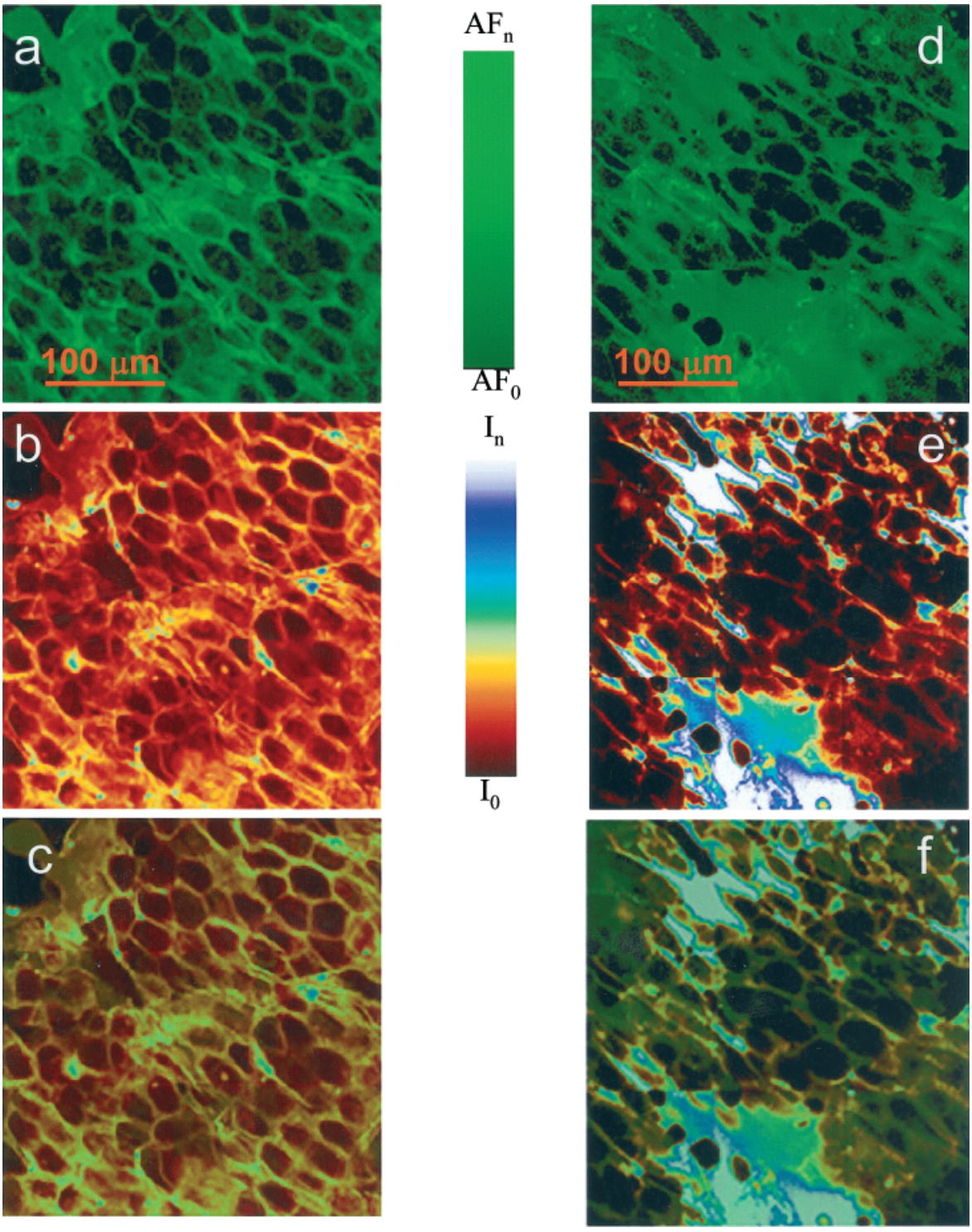

Figure 1. Visualization of the fluorescence intensity of: (*a*) the skin autofluorescence (green DHTPM channel); (*b*) the RBHE model drug intensity (red DHTPM channel); and (*c*) the model drug signal-autofluorescence overlay for the control case, at the same skin spatial coordinates. The corresponding images for the chemical enhancer (oleic acid) case are shown in (*d*), (*e*), and (*f*), respectively. The skin autofluorescence intensity is depicted by the green color bar, where increasing intensities correspond to brighter green colors. $AF_0 = 0$ counts per pixel, whereas $AF_n = 100$ counts per pixel. The model drug intensities are reflected in the red scale color bar, where regions in black indicate low model drug concentration and regions of high model drug concentration are represented by white. The intensities displayed for the RBHE model drug range from $I_0 = 0$ counts per pixel to $I_n = 1000$ counts per pixel.

overlap of the green and the red channels, shown in **Fig 1**(*f*), indicates confinement of the RBHE signal position to the intercellular region defined by the skin autofluorescence image (**Fig 1***d*). Furthermore, the oleic acid induced formation of the hydrophobic drug microdomains are observed at the upper and at the lower bright, white, regions of **Fig 1**(*e*). Compared with the control case (**Fig 1***b*), these microdomains observed in the enhancer case contribute to increased heterogeneity in the model drug spatial distribution. A comparison of the skin autofluorescence (**Fig 1***d*) with the oleic acid-induced

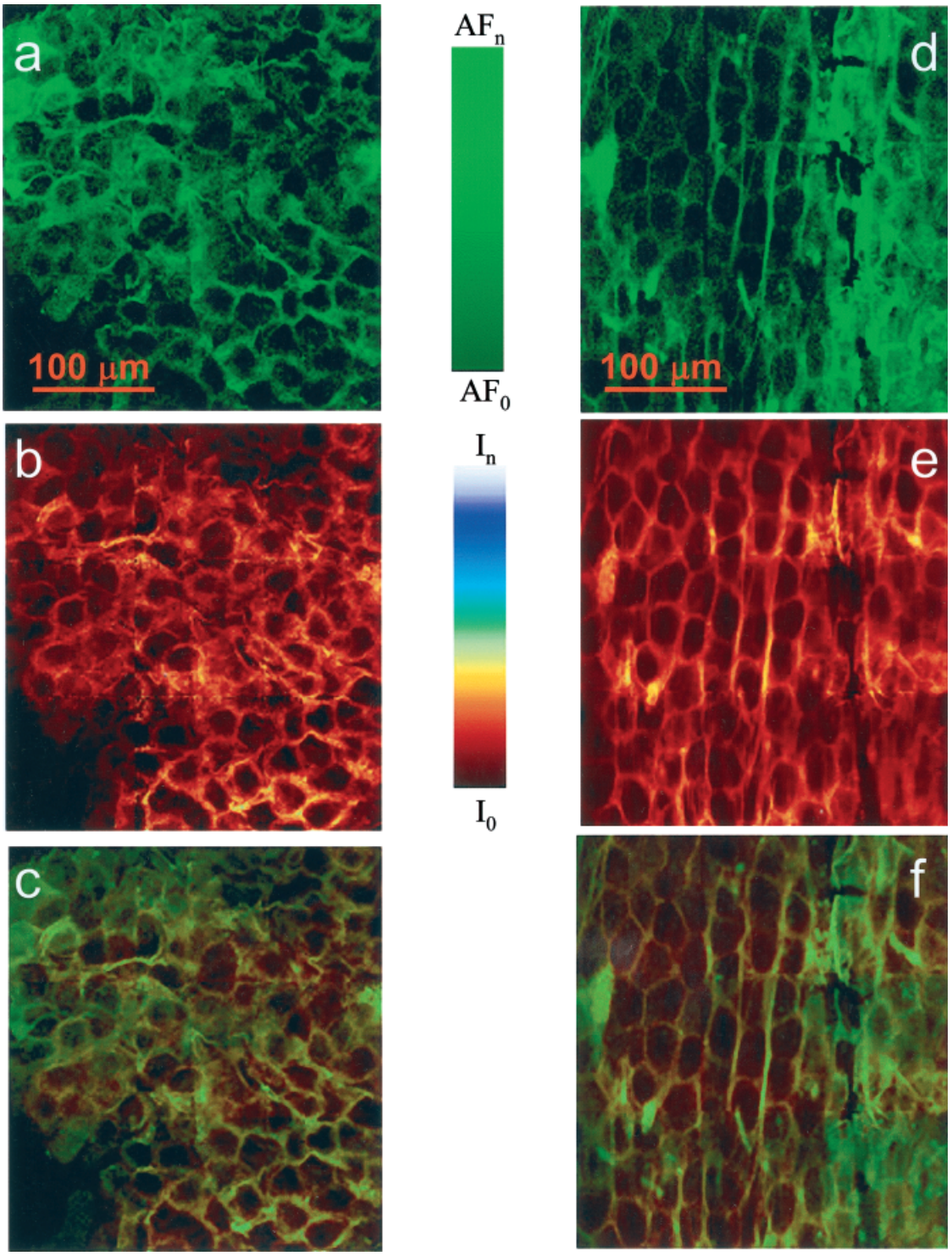

Figure 2. Visualization of the fluorescence intensity of: (*a*) the skin autofluorescence (green DHTPM channel); (*b*) the SRB model drug intensity (red DHTPM channel); and (*c*) the model drug signal-autofluorescence overlay for the control case, at the same skin spatial coordinates. The corresponding images for the chemical enhancer (oleic acid) case are shown in (*d*), (*e*), and (*f*), respectively. $AF_0 = 0$ counts per pixel, whereas $AF_n = 50$ counts per pixel. The range of SRB model drug intensities shown by the color bar range from $I_0 = 0$ counts per pixel to $I_n = 200$ counts per pixel (in panel b) and $I_0 = 0$ counts per pixel to $I_n = 1000$ counts per pixel (in panel e).

hydrophobic model drug spatial distribution (**Fig 1*e***) indicates a decrease in the model drug intracorneocyte penetration with respect to the control case.

Hydrophilic model drug (SRB) **Figure 2**(***a***) shows the SC autofluorescence signal for the hydrophilic model drug (SRB) control case. The corneocytes are the dark polyhedral regions surrounded by the green autofluorescence of the SC intercellular region. The similarity in skin autofluorescence intensity distributions for the hydrophobic model drug (**Fig 1*a***) and for the hydrophilic model drug (**Fig 2*a***) control cases indicates that the intrinsic SC autofluorescence is independent of model drug specific penetration pathways. The fluorescent model drug spatial distributions can therefore be characterized relative to these maps of the intrinsic skin structural features.

The SRB model drug spatial distribution shown in **Fig 2**(***b***) further highlights the intercellular diffusion pathway specific to the physicochemical properties of the hydrophilic fluorescent

model drug. As observed in the wide-area visualization of hydrophilic model drug SRB distributions reported in a previous paper (Yu *et al*, 2002), SRB lies primarily within the intercellular region. The overlapping of the fluorescence signals from the green and the red channels shown in **Fig 2(*c*)** further demonstrates that the SRB model drug spatial distribution is primarily located within the intercellular region defined by the skin autofluorescence. The appearance of SRB model drug intensity within the corneocyte region provides evidence for hydrophilic model drug penetration into the corneocyte region. As described earlier for the RBHE-control case, the SRB intracorneocyte diffusion, visualized in **Fig 2(*b*)**, may be attributed to the model drug concentration difference between the primary hydrophilic model drug transport pathway of the intercellular region and the model drug-deficient corneocyte regions.

In the presence of oleic acid chemical enhancer action, increased hydrophilic model drug intensities were visualized within the corneocyte region. Compared with the corresponding autofluorescence signals, the oleic acid-induced SRB spatial distribution detected in the red channel (see **Fig 2*e***) highlights a continuous phase that is broader than the one detected in the green channel (see **Fig 2*d***). Overlapping the signals detected in the red and the green channels indicates the extent of SRB intracorneocyte penetration (**Fig 2*f***), where the fluorescence signal detected through the red channel extends into the corneocyte regions outlined by the green channel.

A quantification of the observations made above is presented below.

Linear image deconstruction of intracorneocyte model drug intensity distributions For each skin sample, **Figs 3 and 4** capture the linear deconstruction paths examined within the context of the surrounding 150×150 pixel skin area. The fluorescence intensity spectra shown for the RBHE-control, the RBHE-enhancer, the SRB-control, and the SRB-enhancer cases in **Figs 3(*b*), 3(*e*), 4(*b*)**, and **4(*e*)**, respectively, represents the deconstruction of the fluorescence images along one dimension (see *Materials and Methods* above).

Hydrophobic model drug (RBHE) For the RBHE-control in **Fig 3(*b*)**, the model drug intensity spectrum (red line) envelopes the autofluorescence spectrum (green line). The wider model drug intensity spectrum peaks, relative to the referenced peak widths of the corresponding autofluorescence spectrum, indicate that the model drug transport extends beyond the intercellular region defined by the skin autofluorescence intensity spectrum and into the corneocyte structures. Compared with the zero intensity minima exhibited by the skin autofluorescence spectrum, the model drug intensity spectrum minima never approach zero. The model drug intensities detected within the corneocyte regions further corroborate the existence of intracorneocyte model drug penetration potentially driven by the model drug concentration gradient from the intercellular region into the corneocyte region.

In the presence of oleic acid, however, RBHE becomes localized to within the defined intercellular space. The intensity spectra shown in **Fig 3(*e*)** indicate that the widths of the autofluorescence intensity peaks (located at $x = 60$ pixels and at $x = 140$ pixels) extend beyond the corresponding peak widths for the model drug intensity spectrum. In enhancing transdermal transport of the hydrophobic model drug, the action of the oleic acid chemical enhancer is observed in the localization of the RBHE distribution, first to the intercellular region, and second, to the larger domains of high model drug intensity (white regions at the top and at the bottom of **Fig 1*e***), referred to earlier as microdomains of model drug distribution.

Hydrophilic model drug (SRB) **Figure 4(*b*)** shows the SRB-control sample intensity spectrum (red line), corresponding to the white rectangle highlighted in **Fig 4(*a*)**, and the autofluorescence spectrum (green line), corresponding to the white rectangle highlighted in **Fig 4(*c*)**. In **Fig 4(*b*)**, the SRB-control autofluorescence spectrum (green line) exhibits two major peaks at $x = 21$ pixels and at $x = 103$ pixels, with minor peaks at $x = 56$ pixels and at $x = 150$ pixels. These four peaks correspond to the positions of the intercellular regions shown in the white rectangle demarking the linear path evaluated in the corresponding skin autofluorescence image (**Fig 4*c***).

The SRB model drug intensity spectrum peak widths (see red line in **Fig 4*b***) are greater than those corresponding to the skin autofluorescence peaks (see green line in **Fig 4*b***) at the four x-coordinates noted. This difference between the model drug intensity and the skin autofluorescence peak widths indicates that the model drug does penetrate into the corneocyte region, although not to the same extent as for the SRB-enhancer case (described below). The minima corresponding to the SRB-control intensity spectrum in **Fig 4(*b*)** (see red line at $x = 40$ and 75 pixels) do reach the zero intensity value as the spatial position approaches the corneocyte center and away from the intercellular region. The additional peak detected only for the model drug intensity at $x = 120$ pixels provides evidence of model drug penetration into the corneocyte region. The peak-to-peak region of the autofluorescence spectrum (see green line in **Fig 4*b***) from $x = 103$–150 pixels outlines the outer bounds of a corneocyte. The model drug intensity peak at $x = 120$ pixels, as well as the nonzero model drug intensities detected within the corresponding corneocyte region (see red line in **Fig 4*b*** from $x = 103$–150 pixels), indicate model drug penetration within this corneocyte region. Compared with the differences between the hydrophobic model drug peak widths and their corresponding autofluorescence peak widths, the hydrophilic model drug control case displays less intracorneocyte diffusion.

The oleic acid-induced increase in the penetration of the hydrophilic model drug (SRB) into the corneocyte region is observed in the spectra shown in **Fig 4(*e*)**, in which the model drug peak widths far exceed the autofluorescence peak widths that outline the boundary of the intercellular region. The oleic acid-induced increased partitioning of SRB into the SC intercellular region, which was quantified previously (Yu *et al*, 2001, 2002), increases the model drug concentration in the intercellular region. The drop in model drug intensity (red line in **Fig 4*e***) about the peak maximum reflects the concentration gradient driving SRB diffusion into the corneocytes. In contrast to its effect on the hydrophobic model drug localization to the intercellular region, the increased concentration of SRB in the intercellular region contributes to the oleic acid-induced intracorneocyte penetration observed in **Fig 4(*d*)**, where the model drug intensity does not drop to zero in the corneocyte regions.

Based on the visual elucidation of transport pathways through the decomposition of the skin autofluorescence signals from the model drug fluorescence signal, oleic acid was observed to increase intracorneocyte penetration for the hydrophilic model drug and to localize hydrophobic model drug diffusion to either the intercellular region or to the larger domains ("pools") of high model drug intensity.

Implications of the role of corneocyte diffusion on transdermal transport The oleic acid-induced increase in SRB lipid to corneocyte partitioning is observed in the model drug diffusion into the corneocytes. The availability of corneocyte diffusion as a secondary pathway suggests that the constraints to transdermal transport via lateral diffusion through the tortuous intercellular multilamellae no longer hold. Therefore, the oleic acid-induced increase in SRB model drug diffusion into the corneocytes remains consistent with earlier findings that the hydrophilic model drug vehicle to SC partitioning is the rate-limiting step (Yu *et al*, 2002). Furthermore, the hydrophobic model drug rate-limiting step of

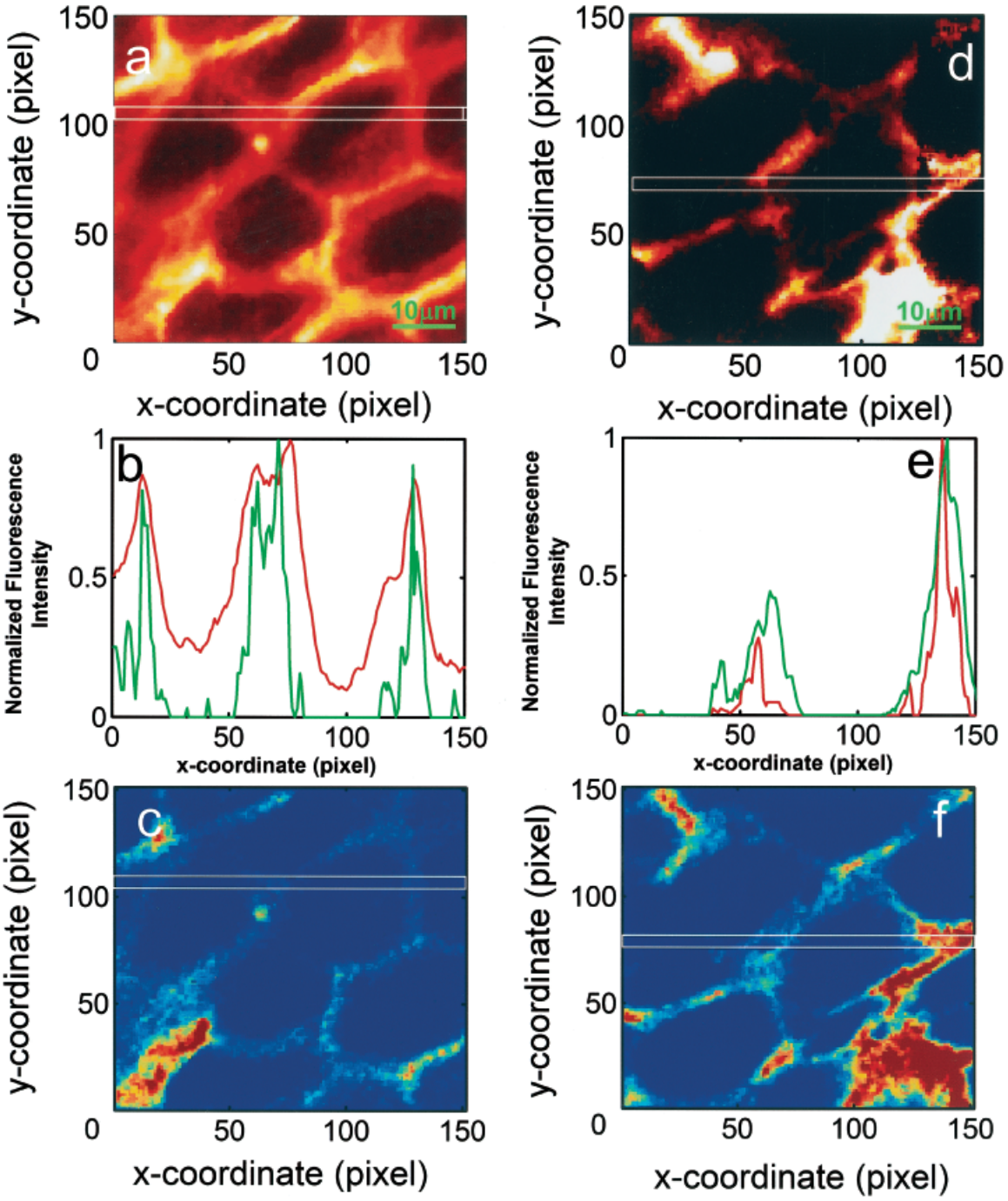

Figure 3. Peak-width image analysis of the hydrophobic model drug (RBHE) intensity spectrum. For the control case, the linear fluorescence intensity deconstruction regions are demarked by the white rectangles in the images of the RBHE model drug spatial distribution, shown in (*a*), and of the corresponding skin autofluorescence signal, shown in (*c*). The green and the red lines in (*b*) represent the skin autofluorescence and the model drug intensity spectra, respectively. For the chemical enhancer (oleic acid) case, the white rectangles in (*d*) and (*f*) show the linear fluorescence intensity deconstruction regions for the images of the model drug spatial distribution and of the skin autofluorescence, respectively. The green and the red lines shown in (*e*) depict the intensity spectra for the skin autofluorescence and for the model drug, respectively. See the text for details.

lateral diffusion coincides with the oleic acid-induced localization of the hydrophobic model drug to domains within the intercellular region. This conclusion remains consistent with the transport hindrance presented by the tortuous lipid multilamellae region for the hydrophobic model drugs established earlier by Johnson *et al* (1997), and more recently Yu *et al* (2002).

For the hydrophobic model drug, the model drug localization to the intercellular region, as well as to discrete domains within the SC, could be attributed to the inherent model drug preference for the oily environment of the lipoidal region and the inherent model drug dislike for the hydrophilic corneocyte interior. Therefore, the oleic acid is observed to increase the hydrophobic model drug solubility in the lipid region, while decreasing the hydrophobic model drug penetration into the corneocyte region. The increased model drug concentrations in the lipoidal region of the SC, resulting from increased model drug partitioning, are localized to the intercellular region such that hydrophobic model drug diffusion is confined to lateral diffusion.

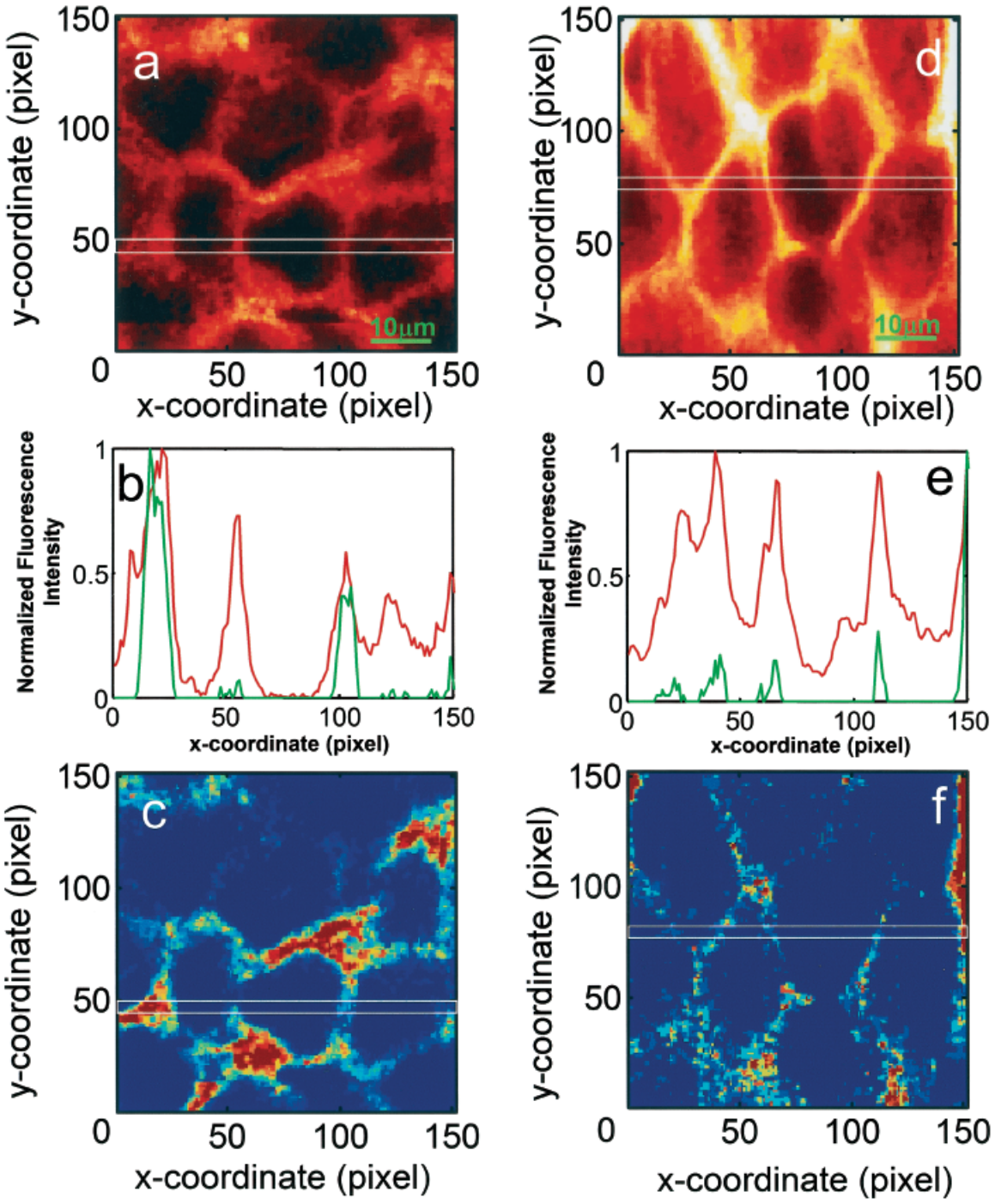

Figure 4. Peak-width image analysis of the hydrophilic model drug (SRB) intensity spectrum. For the control case, the linear fluorescence intensity deconstruction regions are outlined by the white rectangles in the images of the SRB model drug spatial distribution, shown in (*a*), and of the corresponding skin autofluorescence signal, shown in (*c*). The green and the red lines in (*b*) represent the skin autofluorescence and the model drug intensity spectra, respectively. For the chemical enhancer (oleic acid) case, the white rectangles in (*d*) and (*f*) show the linear fluorescence intensity deconstruction regions for the images of the model drug spatial distribution and of the skin autofluorescence, respectively. The green and the red lines shown in (*e*) depict the intensity spectra for the skin autofluorescence and for the model drug, respectively. See the text for details.

For the hydrophilic model drug, however, a different mechanism of transport enhancement was observed. The oleic acid-induced increases in hydrophilic model drug partitioning into the SC lipid multilamellar region drives the hydrophilic model drug from the lipid region into the hydrophilic corneocyte interior. Whereas circumventing transport into the corneocytes promoted hydrophobic model drug transport, transport enhancement for the hydrophilic model drug resulted in increased intracorneocyte diffusion.

CONCLUSIONS

The application of DHTPM to delineate the oleic acid-induced changes in the permeant transdermal pathways has been introduced to elucidate the mechanisms of chemical enhancer action. Oleic acid was found to induce increases in the SRB intracorneocyte diffusion and in the localization of the RBHE model drug diffusion to the intercellular region.

Although the extent of lipid to corneocyte partitioning depends, in part, on the specific physicochemical properties of the

hydrophobic and the hydrophilic model drugs, the mechanistic insight provided here poses the question of how localizing the chemically induced enhancement of transdermal permeant diffusion to the intercellular region may further increase the skin permeabilities to hydrophilic permeants currently achieved with well-known, effective chemical enhancer formulations. The dual function of the corneocytes in the scheme of chemically induced transdermal transport warrants further analyses. In particular, the precise role of intracorneocyte diffusion in enhancing or hindering transport remains to be elucidated.

This research was supported by a National Institutes of Health grant GM 44884.

REFERENCES

Diaspro A: Introduction to two-photon microscopy. *Microsc Res Techn* 47:163–164, 1999

Gerritsen HC, de Grauw CJ: Imaging of optically thick specimen using two-photon excitation microscopy. *Microsc Res Techn* 47:206–209, 1999

Golden GM, Guzek DB, Harris RR, McKie JE, Potts RO: Lipid thermotropic transitions in human stratum corneum. *J Invest Dermatol* 86:255–259, 1986

Golden GM, McKie JE, Potts RO: Role of stratum corneum lipid fluidity in transdermal drug flux. *J Pharm Sci* 76:25–28, 1987

Gonzalez S, Zonios G, Ngyugen BC, Gillies R, Kollias N: Endogenous skin autofluorescence is a good marker for objective evaluation of comedolysis. *J Invest Dermatol* 115:100–105, 2000

Grewal BS, Naik A, Irwin WJ, Gooris G, de Grauw CJ, Gerritsen HG, Bouwstra JA: Transdermal macromolecular delivery. Real-time visualization of iontophoretic and chemically enhanced transport using two-photon excitation microscopy. *Pharm Res* 17(7):788–795, 2000

Heisig M, Lieckfeldt R, Wittum G, Mazurkevich G, Lee G: Non steady-state descriptions of drug permeation through stratum corneum.1. The biphasic brick-and-mortar model. *Pharm Res* 13:421–426, 1996

Johnson ME, Blankschtein D, Langer R: Evaluation of solute permeation through the stratum corneum: Lateral bilayer diffusion as the primary transport mechanism. *J Pharm Sci* 86:1162–1172, 1997

Kim KH, Buehler C, So PTC: High-speed, two-photon scanning microscope. *Appl Optics* 38:6004–6009, 1999

Kollias N, Gillies R, Moran M, Kochevar IE, Anderson RR: Endogenous skin fluorescence includes bands that may serve as quantitative markers of aging and photoaging. *J Invest Dermatol* 111:776–780, 1998

Lopez O, Cocera M, Walther P, de la Maza A, Coderch L, Parra JL: Octyl glucoside as a tool to induce structural modifications in the stratum corneum. *Colloid Surf A-Physicochem Eng Asp* 168:115–123, 2000a

Lopez O, Walther P, Cocera M, de la Maza A, Coderch L, Parra JL: Structural modifications in the stratum corneum by effect of different solubilizing agents: a study based on high-resolution low-temperature scanning electron microscopy. *Skin Pharmacol Appl Skin Physiol* 13:265–272, 2000b

Masters BR, So PTC, Gratton E: Multiphoton excitation fluorescence microscopy and spectroscopy of in vivo human skin. *Biophys J* 72:2405–2412, 1997

Masters BR, So PTC, Gratton E: Optical biopsy of in vivo human skin: Multiphoton excitation microscopy. *Lasers Med Sci* 13:196–203, 1998

Matoltsy AG: Keratinization. *J Invest Dermatol* 67:20–25, 1976

Na R, Stender I-M, Ma L, Wulf HC: Autofluorescence spectrum of skin: Component bands and body site variations. *Skin Res Technol* 6:112–117, 2000

Na R, Stender I-M, Henriksen M, Wulf HC: Autofluorescence of human skin is age-related after correction for skin pigmentation and redness. *J Invest Dermatol* 116:536–540, 2001

Soeller C, Cannell MB: Two-photon microscopy. Imaging in scattering samples and three-dimensionally resolved flash photolysis. *Microsc Res Techn* 47:182–195, 1999

Yamashita F, Koyama Y, Kitano M, Takakura Y, Hashida M: Analysis of in vivo skin penetration enhancement by oleic acid based on a two-layer diffusion model with polar and nonpolar routes in the stratum corneum. *Int J Pharm* 117: 173–179, 1995

Yoneto K, Li SK, Higuchi WI, Shimabayashi S: Influence of the permeation enhancers 1-alkyl-2-pyrrolidones on permeant partitioning into the stratum corneum. *J Pharm Sci* 87:209–214, 1998

Yu B, Dong C-Y, So PTC, Blankschtein D, Langer R: In vitro visualization and quantification of oleic acid induced changes in transdermal transport using two-photon fluorescence microscopy. *J Invest Dermatol* 117:16–25, 2001

Yu B, Kim K, So PTC, Blankschtein D, Langer R: Topographic heterogeneity in transdermal transport revealed by high-speed two-photon microscopy. Determination of representative skin sample sizes. *J Invest Dermatol* 118: 1085–1088, 2002